Controlling of crystal size and optical band gap of CdO nanopowder semiconductors by low and high Fe contents

**C. Aydın · Omar A. Al-Hartomy · A. A. Al-Ghamdi ·
F. Al-Hazmi · I. S. Yahia · F. El-Tantawy ·
F. Yakuphanoglu**

Abstract The CdO:Fe nanopowder semiconductors were synthesized by the sol–gel calcination for the first time. The structural properties of Fe doped CdO samples were analyzed by AFM and XRD measurements. XRD patterns of the pure and Fe-doped CdO samples reveal that the pure and Fe doped CdO nanopowders are polycrystalline of cubic CdO structure. The crystallite size of undoped and Fe-doped CdO samples is changed unsystematically with a regular increase of Fe content. The optical band gaps of Fe doped CdO samples were determined for the first time by diffused reflectance measurements. The optical band gap of the samples is increased with the increase of Fe dopant inside the host matrix (CdO) up to 15 % followed by a decrease in its value. It is evaluated that Fe doped CdO nanopowder semiconductors can be produced by sol–gel calcination for advanced technological applications

1 Introduction

Oxide-diluted magnetic semiconductors (O-DMS) have been extensively investigated due to interest their magnetic properties for spintronic devices such as spin valves [1] and the discovery of these materials leads to most of experimental and theoretical studies on ferromagnetic materials at room temperature (RT). Up to date, transition-metal doped ZnO materials, which are the most widely studied metal oxide semiconductors, where some Zn atoms are replaced by transition metal ions as considered one of these interesting systems [2, 3], have been extensively studied for DMOSs applications.

Transparent conducting oxide thin films such as tin oxides, indium oxides, doped zinc oxides and cadmium oxides have been received more attention due to their high optical transmittance and low resistivity [4–6]. They are very attractive in optoelectronics applications such as surface acoustic wave device, varistors, gas sensors, solar cell technology and transparent conducting electrodes [7, 8]. In particular, cadmium oxide is a promising material for solar cell applications due to its high electrical conductivity and optical transmittance in the visible region of the solar spectrum [9–11]. Pure and metal doped cadmium oxide (CdO) have been used in a wide range of optoelectronic applications like transparent conducting oxide (TCO), solar cells,

C. Aydın
Department of Metallurgical and Materials Engineering,
Firat University,
Elazığ, Turkey

O. A. Al-Hartomy
Department of Physics, Faculty of Science, Tabuk University,
Tabuk 71491, Saudi Arabia

O. A. Al-Hartomy · A. A. Al-Ghamdi · F. Al-Hazmi
Department of Physics, Faculty of Science,
King Abdulaziz University,
Jeddah 21589, Saudi Arabia

I. S. Yahia
Department of Physics, Faculty of Education,
Ain Shams University,
Roxy, Cairo, Egypt

F. El-Tantawy
Department of Physics, Faculty of Science, Suez Canal University,
Ismailia, Egypt

F. Yakuphanoglu (✉)
Physics Department, Faculty of Science, Firat University,
Elazig, Turkey
e-mail: fyhan@hotmail.com

smart windows, and optical communications, flat panel display, photo-transistors, as well as other type of applications like IR heat mirror, gas sensors, low-emissive windows and thin-film resistors etc. [4–8]. The applications based on pure and metal doped CdO can be controlled through the doping process with different types of metallic ions [12, 13].

In previous studies on metal doped CdO such as ions like F, Mn, Dy and Sn [14–18], the dopants increase its free electrons concentration and electrical conductivity. Undoped and doped CdO thin films have been obtained by different techniques [19] such as reactive sputtering (RS) [6], ion beam sputtering [20], activated reactive evaporation [21], chemical bath deposition [22], spray pyrolysis [23], metalorganic chemical vapor deposition [24], and sol–gel (SG) [25]. CdO single crystals have been grown by metalorganic molecular-beam epitaxy [26] and vapor phase reaction [27]. We have evaluated that Sol gel is an attractive synthetic method to prepare metal oxide materials, which are used in a wide variety of fields such as ceramics, sensors, catalysts, optics, electronics and thin films. Thus, sol gel synthesis of materials is an important way to obtain high quality nanopowders for various technological applications. It was observed that with doping by different types of metallic ions, the physical properties of CdO material could be controlled for different technological applications. CdO doped with In, Sn, Al, Sc, and Y, improves its n-type conductivity and increases the optical band gap. Our previous work [28] is based on the preparation and characterization of undoped and Al-doped CdO powder nanostructures via sol–gel calcinations method. Our doping of CdO with transition metals or magnetic ions introduces magnetic properties resulting dilute magnetic oxide semiconductors. According to our knowledge, only A.A. Dakhel [29] studied the structural, optical, and dc-electrical properties of Fe-doped CdO films prepared by vacuum system.

Our work is continuing on the preparation and characterization of CdO doped with magnetic metals to standup their characterization for the advanced technological applications. Up to our knowledge, there is a few works on the preparation and characterization of CdO doped with Fe. In present study, we have investigated the influence of Fe doping on structure and optical properties of CdO nanopowders. Pure and Fe doped CdO were synthesized by sol–gel calcinations process. X-ray diffraction patterns and AFM micrographs were used to study the structure properties of pure and Fe-doped CdO. Optical properties were characterized by diffused reflectance as a new method for investigation the nanopowder samples.

2 Experimental details

2.1 Preparation of the samples

For preparation of CdO powder samples, the schematic diagram of sol gel process is given in Fig. 1. Undoped and
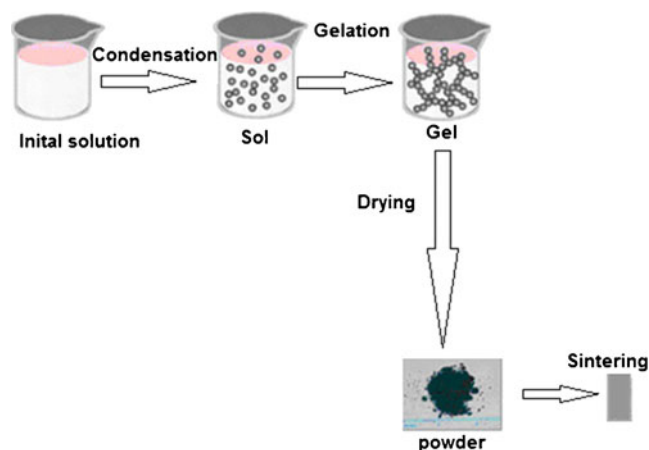
Fig. 1 Schematic diagram of sol gel process for production nanopowders

Fe–doped CdO were prepared by sol–gel route method as follows: Undoped CdO precursor solution was prepared by the following procedures mentioned before [28]: i) the cadmium acetate was dissolved in 2-methoxyethanol (MTE) (0.5 M) at a constant magnetic stirring for 10 min and then, monoethanolamine (0.5 M) (C_2H_7NO, MEA) as stabilizer was added to the solution during the stirring, ii) the solution was stirred constantly for 2 h. CdO precursor containing Fe-dopants were prepared as follows: (0.5 M) cadmium acetate and (0.5 M) with different percents (5, 10, 15 and 20 %) iron (III) chloride ($FeCl_3.6H_2O$), were dissolved in MTE for 10 min. Afterwards, MEA was added drop by drop with continuous stirring and the final solution was stirred for 2 h at 60 °C. The obtained gels were calcinated in a tube furnace for 5 h at 400 °C, respectively. The obtained powders samples were prepared in the disc form.

2.2 Characterization

X–ray diffraction patterns of the prepared samples were obtained with a D8 BRUKER X–Ray diffractometer using CuKα radiations ($\lambda=1.54059$ Å). The structural properties of the powder samples were investigated by Park System XE-100E atomic force microscopy (AFM). The diffuse reflectance spectra of the investigated samples were performed using a Shimadzu UV–VIS-NIR 3600 spectrophotometer using an integrating sphere attachment.

3 Results and discussion

3.1 Structural properties of pure and Fe-doped CdO nanostructure materials

XRD patterns of the pure and Fe-doped CdO nanopowders are shown in Fig. 2(a) and these patterns reveal

Fig. 2 (a). X-ray diffraction patterns of (a) udoped CdO, (b) 5 %, (c) 10 %, (d) 15 % and (e) 20 % Fe-doped CdO nanopowders. (b). The variation of the intensity ratios of (111)/(200) with different Fe concentration
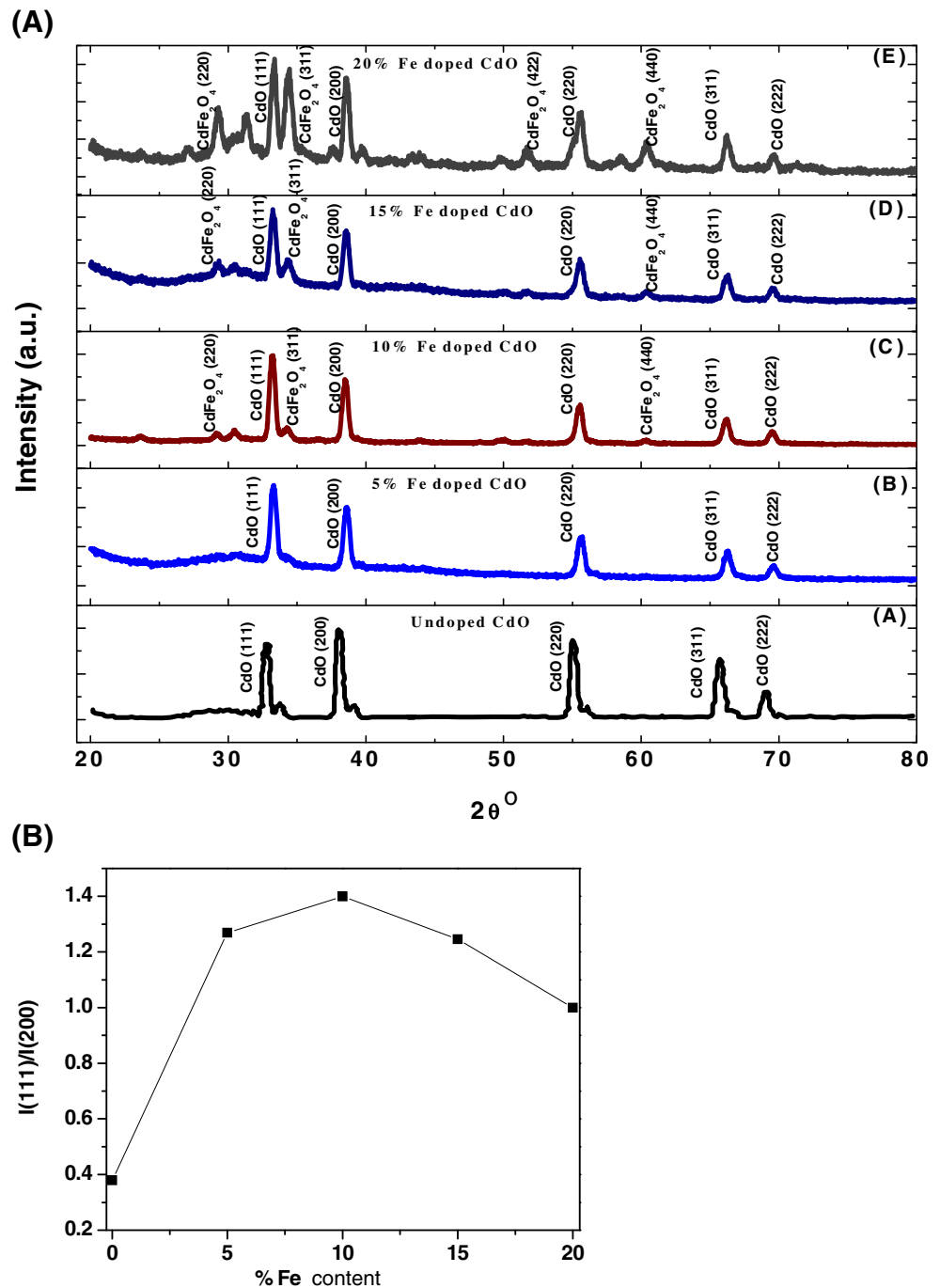
that the prepared nanopowders of pure and Fe doped CdO are polycrystalline of cubic CdO structure. The obtained data are in good agreement with the JCDPS No.78-0653 [30]. The variation of intensity ratios of (111)/(200) with various Fe concentration is shown in Fig. 2(b). It is clear that the intensity ratio of (111)/(200) increases up to 10 % Fe doped CdO and then fall down, which is influenced by present of the second phase $CdFe_2O_4$. For undoped and low concentration of 5 % Fe doped CdO, there is no other phase exhibiting

CdO. As seen in Fig. 2(a), $CdFe_2O_4$ phase is formed for high Fe contents and the intensity of its is increased with increasing Fe doping. This confirms that the high Fe contents change the structure of CdO sample. This means that Fe ions replace inside the host CdO. Although the $CdFe_2O_4$ phase appears in XRD patterns, but CdO phase is the predominant phase inside the investigated samples.

X-ray diffraction results confirm that the predominant phase is CdO inside these samples. The mean value of

the lattice constant a was obtained from interplaner distance of d_{hkl} value of the (111) and (200) peaks using the following equation [31]:

$$d_{hkl} = \frac{a}{\sqrt{h^2 + k^2 + l^2}} \qquad (1)$$

The mean value of the calculated lattice constant a for the undoped and Fe-doped CdO is approximately equals 4.698 Å. The obtained data is in good agreement with JCDPS card No. 78-0653 [30] which equals to 4.725 Å.

X-ray diffraction measurements were used to determine the structural characteristics of undoped and Fe-doped CdO. The average crystallite size of the CdO samples can be calculated from Scherrer's equation by means of full width at half maximum (FWHM) from XRD patterns [32]:

$$D = \frac{0.9\lambda}{\beta \cos\theta} \qquad (2)$$

where β is the full-width at half maximum of the XRD peak appearing at the diffraction angle θ. The crystallite size of undoped and Fe-doped CdO samples is given in Table 1. It is clear from Table 1 that the average crystallite size is changed unsystematically for a regular increase of iron concentration.

Accordingly, some XRD parameters which are the dislocation density δ, the strain ε and the texture coefficient T_c to obtain more information about the structure properties of undoped and Fe-doped CdO nanopowders can be determined using the following equations [33–36]:

$$\delta = \frac{n}{D^2} \qquad (3)$$

$$\varepsilon = \frac{\beta \cos\theta}{4} \qquad (4)$$

The values of dislocation density δ and the strain ε of (111) and (200) planes for undoped and Fe-doped CdO samples are given in Table 1. As seen in Table 1, the dislocation density and strain values of the samples are decreased up to 15 % Fe content and are increased. It is evaluated that these parameters will have an important effect on optical parameters of the samples.

AFM micrographs were used to characterize the structural properties of undoped and Fe doped CdO nanopowders via two (2D) and three (3D) dimensional scales. The AFM images of 2D ($40 \times 40 \, \mu m^2$), inset: 2D ($5 \times 5 \, \mu m^2$) and (3D) dimensional for pure and Fe doped CdO nanopowders are shown in Fig. 3. As seen in Fig. 3, the samples are consisted of nanoparticles in clusters. The type of nanoparticles is like spherical. The diameters of clusters grain size of undoped are given in Table 1. As seen in Table, these parameters are changed with Fe dopant. This suggests that the crystal size of the CdO materials can be controlled by Fe dopant content.

3.2 Determination of optical constants of pure and Fe-doped CdO nanostructure samples

For determination of optical band gap and optical constant of pure and Fe-doped CdO nanostructure powders, we have used the diffuse reflectance spectroscopy. Diffuse Reflectance is widely used in UV–VIS and infrared spectroscopy devices. When incident light strikes a surface, the light that penetrates is reflected in all directions and this is called diffuse reflectance [37]. As the light that leaves the surface has passed through a thin layer of the reflecting material, its wavelength content will have been modified by the optical properties of the matrix. Consequently, the wavelength and intensity distribution of the reflected light will contain structural information on the materials.

Diffuse Reflectance Spectroscopy is a method for the investigation of the quality of the sample, but a special attention must be paid to the theoretical limitations imposed to the system under investigation to obtain a correct qualitative and quantitative interpretation of the experimental data [38, 39]. This method can offer information on the absorption properties of bulk and thin films samples [40, 41] and also on the radiation multiple scattering process in strongly absorbing systems.

Diffuse reflectance studies don't require any sample preparation or a specific surface finish. Materials in their usual form can be characterized by diffuse reflectance spectroscopy. Diffuse Reflectance Spectroscopy can be applied for different kind of materials. Through our work, the optical constants of undoped and Fe-doped CdO nanostructure

Table 1 Values of crystallite size D, strain ε and the dislocation density δ of pure and 5, 10, 15, 20 % Fe-doped CdO powder nanostructures

Sample	The average crystallite size (nm)	The average Clusters size (nm)	The dislocation density $\delta \times 10^{-5}$	The strain ε, $\times 10^{-3}$		E_g (eV)
				(111)	(200)	
0 % Fe	172	419	3.380	117.547	95.949	1.89 [28]
5 % Fe	166	379	3.629	104.630	101.639	2.09
10 % Fe	168	352	3.543	103.162	97.519	2.12
15 % Fe	171	374	3.428	101.485	97.715	2.28
20 % Fe	153	380	4.272	114.275	93.987	2.08
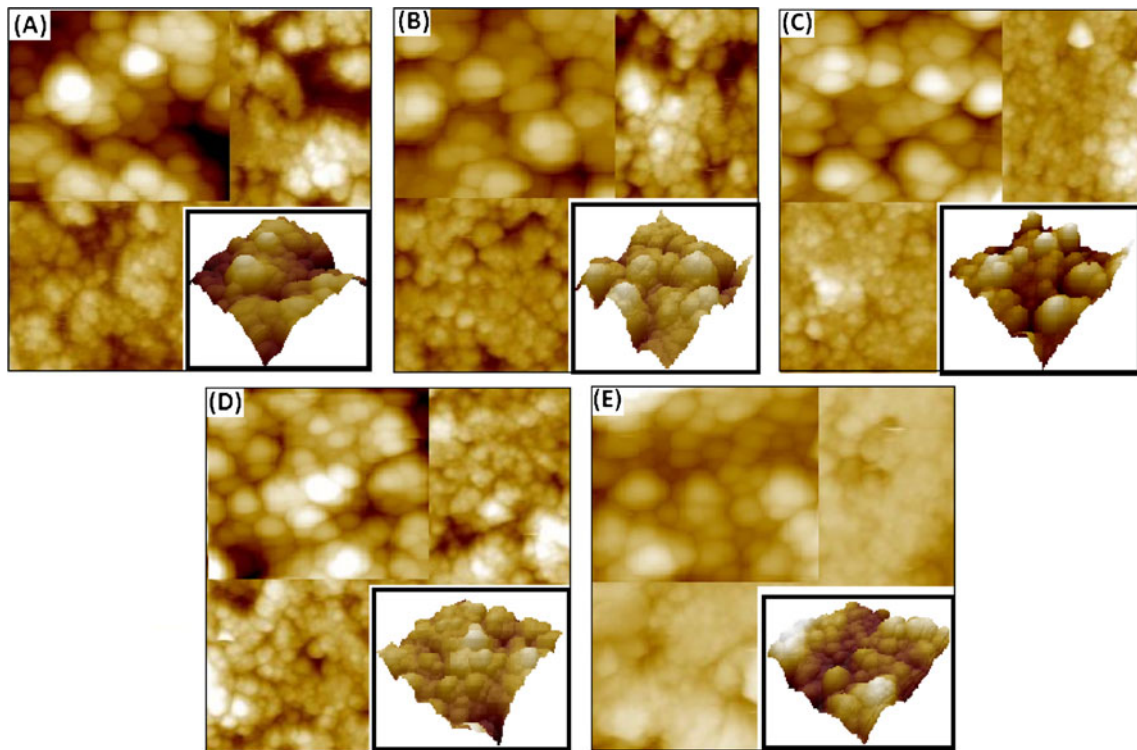
Fig. 3 AFM images of (2D $40 \times 40 \, \mu m^2$). **Insets:** 1- (2D $5 \times 5 \, \mu m^2$) and 2-(3D $1 \times 1 \, \mu m^2$) for (**a**) pure CdO, (**b**) 5 %, (**c**) 10 %, (**d**) 15 % and (**e**) 20 % Fe-doped CdO nanopowders

powders based on the diffuse reflectance spectra were measured as shown in Fig. 4. It is clear that, the reflectance of the samples is increased with increasing wavelengths. In order to determine the precise value of optical band gap of pure and Fe-doped CdO nanostructures, we used optical absorption method on diffuse reflectance. The reflectance
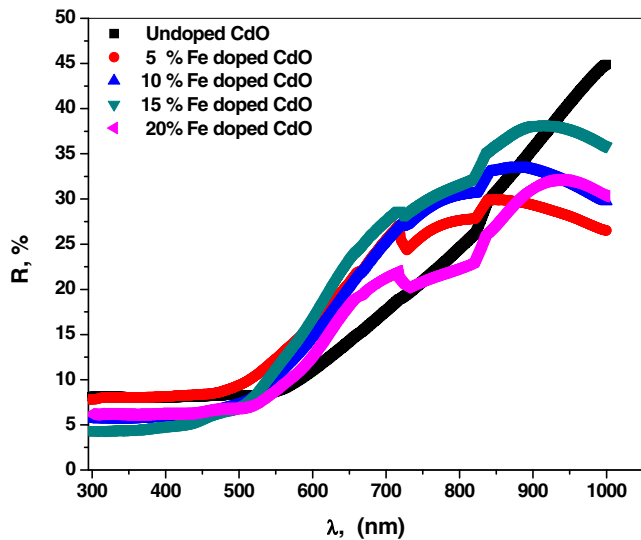
Fig. 4 Diffused reflectance spectrum as a function of wavelength for undoped and (5 %), (10 %), (15 %), and (20 %) Fe-doped CdO nanopowders

values were converted to absorbance by application of Kubelka-Munk function [42–45]. Kubelka-Munk theory is generally used for analyzing the diffuse reflectance spectra obtained from weakly absorbing samples. Kubelka Munk formula can be expressed by the following relation [42–45]:

$$F(R) = \frac{(1-R)^2}{2R} \qquad (5)$$

where R is the diffused reflectance. $F(R)$ is Kubelka–Munk function which corresponds to the absorbance. $F(R)$ values were converted to the linear absorption coefficient by the following relation [45–47].

$$\alpha = \frac{F(R)}{t} = \frac{Absorbance}{t} \qquad (6)$$

where t is the thickness of pure and Fe-doped CdO. It is well known that the optical transitions in semiconductor materials are taken place by direct and indirect transitions. The value of the optical band gap E_g can be calculated using the fundamental absorption, which corresponds to electron excitation from the valance band to conduction band. The optical band gap of the investigated materials can be determined from relation between the absorption coefficient α and the incident photon energy $h\upsilon$ as follows [48, 49]:
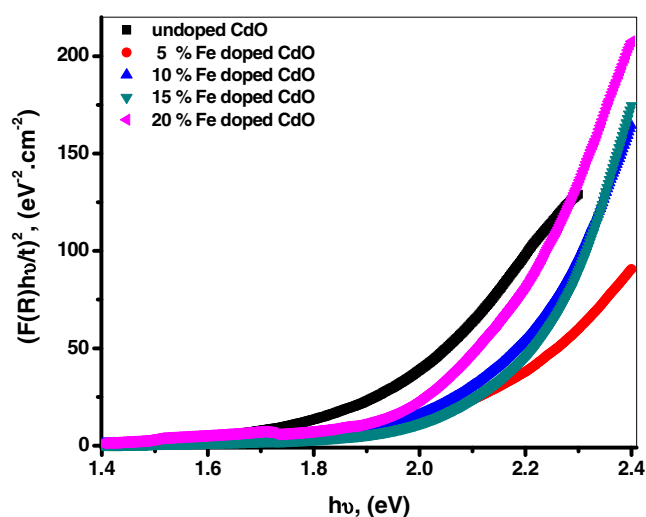
$$(\alpha h\upsilon) = A(h\upsilon - E_g)^n \qquad (7)$$

This equation can be rewritten as [44]

$$(\alpha h\upsilon) = \left(\frac{F(R)h\upsilon}{t}\right) = A\left(h\upsilon - E_g\right)^n, \qquad (8)$$

where A is a constant depending on the transition probability and n is an index that characterizes the optical absorption process. The parameter n has the value 1/2 for the direct allowed transitions and has the value 2 for the indirect allowed transitions. Figure 5 shows the variation of $(F(R)h\upsilon/t)^2$ with photon energy. The optical band gap values for pure and Fe-doped CdO were obtained by extrapolating to the linear portions of these plots to the x-axis (photon energy) i.e. $h\upsilon=0$. The obtained values of the band gap E_g for pure and Fe-doped CdO are given in Table 1. It is clear that the optical band gaps of these samples are increased with the increase of Fe dopants inside the host matrix (CdO) up to 15 % followed by a decrease in its value. It is seen that E_g value of the 20 % Fe doped sample is decreasing drastically when compared 15 % Fe doped CdO sample. This is due to the contribution of secondary phase, $CdFe_2O_4$. As seen in Fig. 2(a), the intensity of CdFe2O4 is higher than that of 15 % Fe doped CdO sample. Furthermore, the obtained E_g value for 20 % Fe doped CdO sample is close to E_g of $CdFe_2O_4$ (E_g=1.97 eV). This confirms that the secondary is an effective parameter in shifting of band gap of the Fe doped CdO samples.

It is expected that the band gap of CdO doped with Fe is due to an increase in carrier concentrations which lead to the Burstein–Moss effect [50]. The shifting in the optical band gap of any material, usually semiconductors, is known as Bursteing–Moss shift due to doping effect. The optical band gaps of the studied pure and 5 % Fe-doped CdO samples are lower than the previously published results about the thin

film samples of these compounds. Up to our knowledge, there is no any reported data about the band gap of pure and Fe-doped CdO nanopowders based on the diffused reflectance calculations.

The normal reflectance for any absorbing material can be expressed through the following equation [51, 52]:

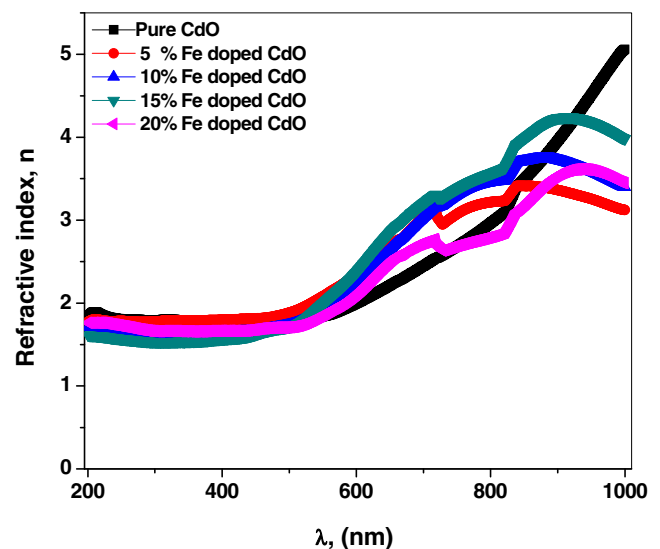$$R = \left(\frac{(n-1)^2 + k^2}{(n+1)^2 + k^2}\right), \qquad (9)$$

For the diffused reflectance, the term k^2 in Eq. 10 is very small for powder materials and thus, Eq. 9 can be rewritten as:

$$R = \left(\frac{(n-1)^2}{(n+1)^2}\right) \qquad (10)$$

Solution of Eq. 10 gives the refractive index of pure and Fe doped CdO as follows [53, 54]

$$n = \left(\frac{1+R}{1-R}\right) + \left(\frac{4R}{(1-R)^2}\right)^{1/2}, \qquad (11)$$

where n is the refractive index and R is the diffused reflectance for the investigated materials. The dependence of the refractive index on the wavelengths for pure and Fe-doped CdO nanopowders is shown in Fig. 6. It is clear that the refractive index is increased with increasing wavelengths followed by a decrease at the higher wavelengths. The refractive index is increased with the increasing Fe dopants up to 15 % followed by a decrease in its value for 20 % Fe dopants. Such behavior is complied with the band gap change of the investigated materials. In this limit range of the wavelengths, the refractive index for pure and Fe-doped

Fig. 5 Plotting of $(F(R)h\upsilon/t)^2$ as a function of the photon energy for pure CdO, (5 %), (10 %), (15 %), and (20 %) Fe-doped CdO nanopowders

Fig. 6 Variation of the refractive index as a function of wavelengths for pure CdO, (5 %), (10 %), (15 %), and (20 %) Fe-doped CdO nanopowders

CdO nanopowders is increased with the increasing wavelengths (anomalous dispersion), through the UV–VIS range followed by a decrease in its values at the higher wavelengths (normal dispersion). Our results cannot compared with thin film samples of CdO and Fe doped CdO prepared by A.A. Dakhel [29]. Our future work has aimed to calculate the optical constants in details for nanopowders materials.

4 Conclusions

The structural and optical properties of the CdO:Fe nanopowders diluted magnetic semiconductors synthesized by sol–gel calcination have been investigated for the first time. AFM and XRD results reveal that the nanopowders of pure and Fe doped CdO are nanomaterials. It was found that the crystal size of the CdO materials is controlled by Fe dopant content. The optical band gaps of the samples were determined using diffused reflectance method. The optical band gaps of CdO samples are increased with the increase of Fe dopants inside the host matrix (CdO) up to 15 % followed by a decrease in its value. The refractive index of the samples were determined using optical reflectance method and the obtained refractive index is increased with the increasing Fe dopants up to 15 % followed by a decrease in its value for 20 % Fe dopants.

The obtained results indicate that the structural and optical properties of CdO nanomaterial can be controlled with low and high content of Fe contents . It is evaluated that the obtained nanopowder semiconductors can be produced by sol–gel calcination for advanced technological applications

References

1. W. Prellier, A. Fouchet, B. Mercey, J Phys Condens Matter **15**, R1583–R1601 (2003)
2. G. Xiong, J. Wilkinson, B. Mischuchk, S. Tüzemen, K.B. Ucer, R.T. Williams, Appl Phys Lett **78**, 1237 (2001)
3. P. Palacios, I. Aguilera, P. Wahnón, Thin Solid Films **518**, 4568–4571 (2010)
4. S.Y. Kim, K. Hong, J.L. Lee, K.H. Choi, K.H. Song, K.C. Ahn, Solid State Electron **52**, 1 (2008)
5. Z.X. Yang, Y. Huang, G.N. Chen, Z.P. Guo, S.Y. Cheng, S.Z. Huang, Sens Actuators B **140**, 549 (2009)
6. S. Aksoy, Y. Caglar, S. Ilican, M. Caglar, Int J Hydrogen Energy **34**, 5191 (2009)
7. J. Santos-Cruz, G. Torres-Delgado, R. Castanedo-Perez, S. Jimenez-Sandoval, J. Marquez-Marín, O. Zelaya-Angel, Sol Energy Mater Sol Cells **90**, 2272 (2006)
8. C.H. Kwon, H.K. Hong, D.H. Yun, K. Lee, S.T. Kim, Y.H. Roh, B.H. Lee, Sens Actuators B **25**, 610 (1995)
9. R. Ferro, J.A. Rodriguez, O. Vigil, A. Morales-Acevado, G. Contreras-Puente, Phys Stat Solidi A **177**, 477 (2000)
10. R.S. Mane, H.M. Pathan, C.D. Lokhande, S.H. Han, Sol Energy **80**, 185 (2006)
11. B.J. Zheng, J.S. Lian, L. Zhao, Q. Jiang, Appl Surf Sci **256**, 2910–2914 (2010)
12. A.A. Dakhel, J Alloys Compd **475**, 51–54 (2009)
13. A.A. Dakhel, Solar Energy **83**, 934–939 (2009)
14. M. Kul, M. Zor, A.S. Aybek, S. Irmak, E. Turan, Thin Solid Films **515**, 8590 (2007)
15. V. Bilgin, I. Akyuz, S. Kose, F. Atay, Semicond Sci Technol **21**, 579 (2006)
16. T. Chen, Q.J. Liu, Z.L. Zhou, Y.D. Wang, Nanotechnology **19**, 095506 (2008)
17. A.A. Dakhel, Sol Energy **83**, 934 (2009)
18. Z.Y. Zhao, D.L. Morel, C.S. Ferekides, Thin Solid Films **413**, 203 (2002)
19. K. Gurumurugan, D. Mangalaraj, Sa.K. Narayandass, J Electron Mater **25**, 765 (1996)
20. T.L. Chu, S.S. Chu, J Electron Mater **19**, 1003 (1990)
21. G. Phatak, R. Lal, Thin Solid Films **245**, 17 (1994)
22. D.M. Carballeda-Galicia, R. Castanedo-Pérez, O. Jiménez-Sandoval, S. Jiménez-Sandoval, G. Torres-Delgado, C.I. Zúñiga-Romero, Thin Solid Films **371**, 105–108 (2000)
23. R. Ferro, J.A. Rodriguez, Thin Solid Films **347**, 295 (1999)
24. Z. Zhao, D.L. Morel, C.S. Ferekides, Thin Solid Films **413**, 203 (2002)
25. D.M. Carballeda-Galicia, R. Castanedo-Pérez, O. Jiménez-Sandoval, S. Jiménez-Sandoval, G. Torres-Delgado, C.I. Zúñiga-Romero, Thin Solid Films **371**, 105–108 (2000)
26. A.B.M.A. Ashrafi, H. Kumano, I. Suemune, Y.W. Ok, T.Y. Seong, J. Cryst, Growth **237–239**, 518–522 (2002)
27. S. Hayashi, Rev Electr Commun Lab **20**, 698 (1972)
28. C. Aydın, H.M. El-Nasser, F. Yakuphanoglu, I.S. Yahia, M. Aksoy, J Alloy Compd **509**, 854 (2011)
29. A.A. Dakhel, Thin Solid Films **518**, 1712–1715 (2010)
30. International Centre for Diffraction Data. JCDPS, PCPDFWIN, v. 2.3; 2002.
31. R.J. Deokate, S.V. Salunkhe, G.L. Agawane, B.S. Pawar, S.M. Pawar, K.Y. Rajpure, A.V. Moholkar, J.H. Kim, J Alloys Compd **496**, 357 (2010)
32. B.D. Cullity, *Elements of x-ray diffraction* (Addison-Wesly, Massachusetts, 1956)
33. W.D. Callister, *Materials science and engineering-an introduction* (Wiley, New York, 1997)
34. D.P. Padiyan, A. Marikini, K.R. Murli, Mat Chem Phys **78**, 51 (2002)
35. K.R. Murali, A. Kalaivanan, S. Perumal, N. Neelakanda Pillai, J Alloys Compd **503**, 350 (2010)
36. C. Barret, T.B. Massalski, *Structure of metals* (Pergamon, Oxford, 1980)
37. http://www.analyticalspectroscopy.net/ap3-11.htm
38. M. Milosevic, S.L. Birets, Appl Spectrosc Rev **37**, 347 (2002)
39. R. Nagarajan, D. Gupta, Infrared Phys Tech **43**, 377 (2002)
40. D.J. Dahm, K.D. Dahm, K.H. Norris, J Near Infrared Spectrosc **10**, 1 (2002)
41. M. Socol, A. Stanculescu, Journal of Optoelectronics and Advanced Materials **8**, 185 (2006)
42. A. Escobedo Morales, E. Sanchez Mora, U. Pal, Rev. Mexic. De Fisica S 53 (2007)
43. V. Senthilkumar, P. Vickraman, R. Ravikumar, J Sol-Gel Sci Technol **53**, 316 (2010)
44. F. Yakuphanoglu, J Alloys Compd **507**, 184 (2010)

45. F. Yakuphanoglu, R. Mehrotra, A. Gupta, M. Munoz, J Appl Polymer Sci **114**, 794 (2009)
46. A.E. Morales, E.S. Mora, U. Pal, Rev Mex Fis **53**(5), 18 (2007)
47. E. Yassitepe, Z. Khalifa, G.H. Jaffari, C.-S. Chou, S. Zulfiqar, M.I. Sarwar, S.I. Shah, Powder Technology **201**, 27 (2010)
48. J.I. Pankove, *Optical processes in semiconductors* (Prentice-Hall, Englewood Cliffs, 1971)
49. O.A. Azim, M.M. Abdel-Aziz, I.S. Yahia, Appl Surf Sci **255**, 4829 (2009)
50. B. Saha, S. Das, K.K. Chattopadhyay, Solar Energy Mater. Solar Cells **91**(311), 1692 (2007)
51. M. Okutan, S. Eren San, O. Köysal, F. Yakuphanoglu, Physica B **362**, 180 (2005)
52. H. Kresse et al., Phys Stat Sol **106**, 89 (1988)
53. N.A. Subrahamanyam, *A textbook of optics*, 9th edn. (Brj Laboratory, Delhi, 1977)
54. S. Ilican, Y. Caglar, M. Caglar, F. Yakuphanoglu, Appl Surf Sci **255**, 2353 (2008)